

The Radio and X-ray Luminous Type Ibc Supernova 2003L

A. M. Soderberg¹, S. R. Kulkarni¹, E. Berger^{2,3,4}, R. A. Chevalier⁵, D. A. Frail⁶, D. B. Fox¹, R. C. Walker⁶

ABSTRACT

We present extensive radio observations of SN 2003L, the most luminous and energetic Type Ibc radio supernova with the exception of SN 1998bw (associated with GRB 980425). Observations from the Very Large Array are well described by a fitting a synchrotron self-absorption model to the emission spectrum. This model implies a sub-relativistic ejecta velocity, $\bar{v} \approx 0.2c$, and a size of $r \approx 4.3 \times 10^{15}$ cm at $t \approx 10$ days. The circumstellar density is suitably fit with a stellar wind profile, $n_e \propto r^{-2}$ and a constant mass loss rate of $\dot{M} \approx 7.5 \times 10^{-6} M_{\odot} \text{ yr}^{-1}$. Moreover, the magnetic field follows $B \propto r^{-1}$ and the kinetic energy of the radio bright ejecta is roughly $E \approx 10^{48}$ erg assuming equipartition of energy between relativistic electrons and magnetic fields. Furthermore, we show that free-free absorption does not contribute significantly to the radio spectrum, since it implies ejecta velocities which are inconsistent with size constraints derived from Very Long Baseline Array observations. In conclusion, we find that although SN 2003L has a radio luminosity comparable to that seen in SN 1998bw, it shows no evidence for a significant amount of energy coupled to relativistic ejecta. Using SN 2003L as an example, we comment briefly on the coupling of ejecta velocity and energy in Type Ibc supernovae.

Subject headings: gamma rays: bursts - radiation mechanisms: nonthermal - radio continuum: general - supernova: individual (SN 2003L)

¹Division of Physics, Mathematics and Astronomy, 105-24, California Institute of Technology, Pasadena, CA 91125

²Observatories of the Carnegie Institution of Washington, 813 Santa Barbara St., Pasadena, CA 91101

³Department of Astrophysical Sciences, Princeton University, Princeton, NJ 08544

⁴Hubble Fellow

⁵Department of Astronomy, University of Virginia, P.O. Box 3818, Charlottesville, VA 22903-0818

⁶National Radio Astronomy Observatory, Socorro, NM 87801

1. Introduction

Radio emission from core-collapse supernovae (SNe) have been sought primarily to study the circumstellar medium (Weiler *et al.* 1986; Chevalier 1998). However, starting with Type Ibc SN 1998bw, associated with the under-luminous gamma-ray burst GRB 980425 (Pian *et al.* 2000; Galama *et al.* 1998; Kulkarni *et al.* 1998), radio observations have also been used a tracer of relativistic ejecta (Kulkarni *et al.* 1998; Li & Chevalier 1999). This event prompted a storm of publications: SN 1998bw was the most luminous radio supernova (at early times), showed strong variability and produced copious gamma-ray emission relative to ordinary SNe Ibc. These data provided the first observational evidence that at least some SNe Ibc are associated with GRBs (e.g. Bloom *et al.* 1999, 2002; Stanek *et al.* 2003, c.f. Price *et al.* 2003).

To further explore the connection between GRBs and SNe Ibc, we began a radio survey of local Type Ibc supernovae. Our survey was motivated by two simple phenomenological questions: (1) What is the prevalence of SN 1998bw-like supernovae?, and (2) Is there a continuum between ordinary SNe and GRBs as traced by their relativistic ejecta?

In Berger *et al.* (2003) we reported the first three years of the survey. We found that most SNe Ibc are not detectable with current radio sensitivity, with limits reaching 10^{-3} that of the peak brightness of SN 1998bw. Clearly, luminous SN 1998bw-like supernovae are rare (less than 3%) and those within an order of magnitude of SN 1998bw are uncommon (less than 10%).

Here, we present radio observations of SN 2003L, the first SN Ibc with a radio luminosity comparable to SN 1998bw. While there is no evidence for mildly-relativistic ejecta, the radio emitting ejecta of SN 2003L are unusually energetic. This discovery suggests the existence of a sub-class of SNe Ibc with similar energetics to SN 1998bw and even weaker central engines, if any.

The organization of this paper is as follows: observations from the Very Large Array (VLA), the Very Long Baseline Array (VLBA) and the *Chandra* X-ray Observatory (CXO) are described in §2 and §3. Preliminary estimates of the energy and velocity are presented in §4. Modeling of the radio light-curves is discussed in Sections 5 and 6 assuming the dominant absorption is from internal synchrotron self-absorption and external free-free absorption, respectively, Modeling of the X-ray emission follows as §7. In the Discussion (§8) we conclude by addressing the nature of SN 2003L.

2. Radio Observations of SN 2003L

2.1. Very Large Array Data

SN 2003L was optically discovered on 2003 January 12.15 UT, offset $9''.0$ W and $1''.5$ N from the center of NGC 3506 (Boles 2003) and at a distance of $d \approx 92$ Mpc (Valenti *et al.* 2003). In our first observation with the Very Large Array⁷ (VLA), on 2003 January 26.2 UT, we detected a radio source coincident with the optical position at $\alpha(\text{J2000}) = 11^{\text{h}}03^{\text{m}}12.3^{\text{s}}$, $\delta(\text{J2000}) = +11^{\circ}04'38.1''$ (± 0.1 arcsec in each coordinate) with flux density of $f_{\nu} = 743 \pm 39 \mu\text{Jy}$ at 8.5 GHz. This, and subsequent observations at 4.9, 8.5, 15.0 and 22.5 GHz, are summarized in Table 1.

All observations were taken in standard continuum observing mode with a bandwidth of 2×50 MHz. We used 3C286 for flux calibration, and for phase referencing we used calibrators J1118+125, J1120+134 and J1103+119. Data were reduced using standard packages within the Astronomical Image Processing System (AIPS).

As seen in Table 1, observations were taken in each of the four VLA configurations. The decreased spatial resolution of the C and D configurations resulted in detection of diffuse host galaxy emission surrounding the supernova, primarily affecting the low (≤ 8.5 GHz) frequency observations (Figure 1). At 8.5 GHz the host galaxy extends 45×45 arcsec, but is resolved away on baselines ≥ 10 k λ . By restricting the UV range to exclude shorter baselines, we measured the flux density of the supernova with minimal contribution from the host galaxy. Measurements at higher frequencies and in other VLA configurations were made by fitting a Gaussian to the SN emission and solving for the integrated intensity.

Figure 2 shows the SN 2003L radio light-curves assuming an approximate explosion date of 2003 January 1.0 UT as derived from optical data (Soderberg *et al.* 2004). The radio light-curves evolve as $f_{\nu} \propto t^{1.2}$ before the peak, exhibit a broad maximum and fade as $f_{\nu} \propto t^{-1.2}$. The spectral index (β with $f_{\nu} \propto \nu^{\beta}$) is observed as $\beta \approx -1.1$ in the optically thin regime (Figure 3).

⁷The Very Large Array and Very Long Baseline Array are operated by the National Radio Astronomy Observatory, a facility of the National Science Foundation operated under cooperative agreement by Associated Universities, Inc.

2.2. Very Long Baseline Array Data

Complimentary to our VLA campaign, we obtained a single observation of SN 2003L using the Very Large Baseline Array (VLBA). The six hour observation began on 2003 March 7.30 UT ($t \approx 65$ days), and was taken in standard continuum mode with a bandwidth of 4×8 MHz centered on the observing frequency of 4.9 GHz. Fringe calibrations were applied using 3C273 and phase referencing was conducted using J1103+1158 at an angular distance of 0.9 degrees from the SN.

We detect SN 2003L at a position of $\alpha = 11^{\text{h}}03^{\text{m}}12^{\text{s}}.3008$, $\delta = +11^{\circ}04'38''.08$ (J2000.0) with a positional uncertainty of 10 mas in each coordinate (Figure 4). We note that these errors are dominated by the positional uncertainty of J1103+1158, assumed to be at $\alpha = 11^{\text{h}}03^{\text{m}}03^{\text{s}}.5299$, $\delta = +11^{\circ}58'16''.61$ (J2000.0). Using the VLBA utilities within AIPS, we find a flux density for the supernova of $F_{4.9 \text{ GHz}} = 848 \pm 64 \mu\text{Jy}$ within the 3.158×1.285 mas beam. We note that there is no emission from the host galaxy at this resolution. At a distance of 92 Mpc, this unresolved VLBA detection places a direct constraint on the size of the expanding ejecta of $r \lesssim 9.1 \times 10^{17}$ cm and an average expansion speed of $\bar{v} \leq 5.4c$ during the first 65 days after the explosion.

3. X-ray Observations with *Chandra*

We observed SN 2003L with the *Chandra* ACIS-S detector beginning at 2003 February 10.15 UT ($t \approx 40$ days). During the 30 ksec observation, we detected 30 ± 6 counts from the supernova (Kulkarni & Fox 2003). For spectral extraction we adopt a source aperture of 2.46 arcsec, which encloses approximately 98% of the flux of an on-axis point-source at 1 keV (the peak of our raw photon counts spectrum). Our aperture correction is therefore minimal by comparison to our $\sim 20\%$ flux uncertainties (see below). Background counts are selected from an annular region extending from 2.46 arcsec to 7.38 arcsec from the source; in general larger background regions are preferred for *Chandra* data analysis but the extended emission from the host galaxy makes a more local selection preferable in this case (see Figure 5).

Schlegel, Finkbeiner & Davis (1998) dust maps give $E(B - V) = 0.021$ mag for the location of SN 2003L. Dickey & Lockman (1990) suggest an average N_{H} of $2.25 \times 10^{20} \text{cm}^{-2}$, while a direct conversion from the Schlegel et al. optical reddening suggests $1.13 \times 10^{20} \text{cm}^{-2}$ (Predehl & Schmitt 1995). We fix N_{H} for our fits at $2.5 \times 10^{20} \text{cm}^{-2}$.

For a power-law spectral fit we find the power-law photon index $\Gamma = 1.53 \pm 0.4$ (range is 0.86 to 2.24 at 90% confidence). For a thermal bremsstrahlung spectral fit we find the plasma temperature has $kT > 1.7 \text{keV}$ at 90% confidence, with a best-fit value of 6.7 keV

that is unconstrained from higher energies. The relatively small number of counts enables satisfactory fits (reduced chi-squared values of $\chi_r^2 \approx 1.3$; 5 degrees of freedom) for both models, with the neutral hydrogen absorption applied to either a power-law or thermal bremsstrahlung continuum.

Our source count rate is 1.0 ± 0.2 cts/ksec in the ACIS-S3 detector. This corresponds to a 0.5–5.0 keV flux for our spectral models of approximately 5.3×10^{-15} erg/cm²/s in either case. Extrapolating to the full 2–10 keV X-ray band, the corresponding fluxes are 9.2×10^{-15} erg/cm²/s for the power law model and 7.6×10^{-15} erg/cm²/s for the thermal bremsstrahlung model. The associated X-ray luminosity is thus $L_{2-10 \text{ keV}} \approx 9.2 \times 10^{39}$ erg/s and 7.2×10^{39} erg/s for the power-law and thermal models, respectively. In comparison with other X-ray supernovae, SN 2003L is among the most luminous ever detected, only a factor of ~ 10 fainter than SN 1998bw at a comparable epoch (Pian *et al.* 2000).

4. Preliminary Constraints

We are interested in the energy and expansion velocity of the ejecta producing the radio emission. As a preliminary constraint, we estimate the brightness temperature, T_B , of SN 2003L and compare it with robust constraints imposed by the Inverse Compton Catastrophe (ICC; Kellermann & Pauliny-Toth 1981). The brightness temperature of a source with angular radius, θ is given by

$$T_B = \left(\frac{c^2}{2\pi k} \right) \left(\frac{f_\nu}{\theta^2} \right) \nu^{-2} \text{ K} \quad (1)$$

Compact sources with $T_B \gtrsim 10^{12}$ K cool rapidly via inverse Compton scattering. As an initial estimate for the physical size of the supernova, we first assume that the optical expansion velocity of 12000 km s⁻¹ (Matheson *et al.* 2003) can be used as an average speed to describe the motion of the radio bright ejecta. Using our approximate explosion date, we estimate the shock radius to be $r \approx 2.9 \times 10^{15}$ cm at $t \approx 28$ days. For an observed flux density of $f_\nu \approx 3.1$ mJy at $\nu \approx 22.5$ GHz, the brightness temperature is $T_B \approx 6.3 \times 10^{11}$ K, just below of the inverse Compton catastrophe (ICC) limit. This exercise provides no evidence for relativistic ejecta, therefore suggesting that SN 2003L expands with a modest sub-relativistic velocity.

For radio sources dominated by synchrotron-self absorption (SSA), the brightness temperature can be further constrained to $T_B < 4 \times 10^{10}$ K. By assuming equipartition between the energy in electrons (ϵ_e) and magnetic fields (ϵ_B), we derive an estimate of the velocity and a lower limit on the kinetic energy of radio emitting material. This approach has been used extensively in discussion of extra-galactic sources and was more recently applied to supernovae (Chevalier 1998; Kulkarni *et al.* 1998). The method requires three observables at

any single epoch: the spectral peak frequency, ν_p , the peak flux density, f_p , and the spectral index of the optically thin emission, $f_\nu \propto \nu^\beta$. Here, $\beta \equiv -(p-1)/2$ for electrons accelerated into a power-law distribution, $N(\gamma) \propto \gamma^{-p}$ above a minimum Lorentz factor, γ_m . Following Kulkarni *et al.* (1998) and Berger, Kulkarni & Chevalier (2002), the angular radius of the radiosphere, θ_{ep} , and the equipartition energy, E_{ep} , are given by

$$\theta_{\text{ep}} \approx 120 \left(\frac{d}{\text{Mpc}} \right)^{-1/17} \left(\frac{f_p}{\text{mJy}} \right)^{8/17} \left(\frac{\nu_p}{1 \text{ GHz}} \right)^{(-2\beta-35)/34} \mu\text{as} \quad (2)$$

$$E_{\text{ep}} \approx 1.1 \times 10^{56} \left(\frac{d}{\text{Mpc}} \right)^2 \left(\frac{f_p}{\text{mJy}} \right)^4 \left(\frac{\nu_p}{1 \text{ GHz}} \right)^{-7} \left(\frac{\theta_{\text{ep}}}{\mu\text{as}} \right)^{-6} \text{ erg.} \quad (3)$$

At $t \approx 30$ days (our first epoch) the peak flux density is $f_p \approx 3.2$ mJy at $\nu_p \approx 22.5$ GHz. Using the observed optically thin spectral index of $\beta \approx -1.1$, Equations 2 and 3 give $\theta_{\text{ep}} \approx 7.7 \mu\text{as}$ implying an equipartition radius of $r_{\text{ep}} \approx 1.1 \times 10^{16}$ cm and an average expansion speed of $\bar{v}_{\text{ep}} \approx 0.15c$. The minimum energy of the ejecta is thus $E_{\text{ep}} \approx 1.5 \times 10^{47}$ erg and the magnetic field is $B_{\text{ep}} \approx 1.1$ G. These constraints alone demand that SN 2003L is among the most energetic Type Ibc supernovae in terms of radio-emitting ejecta, second only to SN 1998bw. We note that additional absorption terms (e.g. free-free absorption) and the inclusion of shocked protons serve to increase the equipartition energy estimate.

Equipartition analyses may also be used to roughly constrain the minimum electron Lorentz factor and the characteristic synchrotron frequency, ν_m . Equating particle kinetic energy across the shock discontinuity, we find

$$\epsilon_e \left(\frac{v}{c} \right)^2 m_p c^2 \approx \bar{\gamma} m_e c^2 \quad (4)$$

where $\bar{\gamma}$ is the average Lorentz factor of the electrons and v is the velocity of the ejecta. Assuming roughly $\bar{\gamma} \approx \gamma_m$ and substituting Equation A6 for γ_m , we derive the following estimate for the characteristic synchrotron frequency, ν_m ,

$$\nu_m \approx \epsilon_e^2 \left(\frac{v}{c} \right)^4 \left(\frac{m_p}{m_e} \right)^2 \left(\frac{eB}{2\pi m_e c} \right) \text{ Hz.} \quad (5)$$

Adopting the values derived from equipartition analyses ($v \approx 0.15c$, $B = 1.1$ G and $\epsilon_e = 0.5$), we find roughly $\nu_m \approx 1$ GHz at $t \approx 30$ days which is below our observing band.

5. Internal Synchrotron Self-Absorption

In the Appendix we present a rigorous formulation of the temporal and spectral evolution of synchrotron emission arising from sub-relativistic supernova ejecta. This prescription, based on the formalism of Frail, Waxman & Kulkarni (2000), is generalized to include the cases where ν_m , is greater than the self-absorption frequency, ν_a , and where $\epsilon_e \neq \epsilon_B$.

The observed flux density and radio spectrum at any single epoch are determined by three parameters: C_f , C_τ and $\nu_{m,0}$. Here, C_f and C_τ are normalization constants of the flux density and optical depth, respectively, while $\nu_{m,0}$ is the value of ν_m at epoch t_0 . The parameters C_f , C_τ and $\nu_{m,0}$ are in turn determined by the values of four physical parameters at $t = t_0$: the magnetic field, B_0 , the shock radius, r_0 , the minimum electron Lorentz factor, $\gamma_{m,0}$, and the ratio of energy densities, $\mathfrak{F}_0 \equiv \epsilon_e/\epsilon_B$. With four physical parameters (B_0 , r_0 , $\gamma_{m,0}$, \mathfrak{F}_0) and only three constraints (C_f , C_τ , $\nu_{m,0}$), we must assume an additional constraint in order to find a unique solution. An additional constraint is obtained by adopting a value for \mathfrak{F}_0 . Inverting the equations for C_f , C_τ and $\nu_{m,0}$ (Equations A13, A14 and A15, respectively) we derive the following expressions for B_0 , r_0 and $\gamma_{m,0}$.

$$B_0 = \left[1.3 \times 10^8 \pi^{15} (2+p)^{-6} (p-2)^{-4} \frac{m_e^{19} c^{21}}{e^{17}} \frac{\eta^4}{\mathfrak{F}_0 d^4} \right]^{1/17} \times C_f^{-2/17} C_\tau^{4/17} \nu_{m,0}^{-2(p-2)/17} \text{ G} \quad (6)$$

$$r_0 = \left[1.5 \times 10^{-2} \pi^{-9} (2+p)^7 (p-2)^{-1} \frac{c}{m_e^8} \frac{\eta d^{16}}{\mathfrak{F}_0} \right]^{1/17} \times C_f^{8/17} C_\tau^{1/17} \nu_{m,0}^{-(p-2)/34} \text{ cm} \quad (7)$$

$$\gamma_{m,0} = \left[3.1 \times 10^{-2} \pi \frac{(2+p)^3 (p-2)^2 \mathfrak{F}_0^2 d^2}{m_e c^2 \eta^2} \right]^{1/17} \times C_f^{1/17} C_\tau^{-2/17} \nu_{m,0}^{(13+2p)/34} \quad (8)$$

Here, we define d as the distance to the supernova and η characterizes the thickness of the radiating electron shell as r/η . We make the standard assumption of a thin shell with $\eta = 10$ (Li & Chevalier 1999; Frail, Waxman & Kulkarni 2000).

5.1. Hydrodynamical Evolution of the Ejecta

Evolutionary models governing the hydrodynamics of the SN ejecta provide additional constraints. As discussed by Chevalier (1996), there are several different models that can be used to describe the hydrodynamic evolution of the ejecta. These models allow the temporal indices, α_r , α_B , α_γ and $\alpha_{\mathfrak{F}}$ to be constrained. Here, we adopt the standard model of Chevalier 1996 for our basic SSA fit.

The first assumption of the standard model is that the hydrodynamic evolution of the ejecta is self-similar across the shock discontinuity. This implies $r \propto t^{\alpha_r}$ with $\alpha_r = (n - 3)/(n - s)$ where n is the density profile of the outer SN ejecta ($\rho \propto r^{-n}$) and s is the density profile of the radiating electrons within the shocked circumstellar medium ($n_e \propto r^{-s}$). In addition, the standard model assumes that the magnetic energy density ($U_B \propto B^2$) and the relativistic electron energy density ($U_e \propto n_e \gamma_m$) scale as the total post-shock energy density ($U \propto n_e v^2$). In this scenario, the magnetic field is amplified by turbulence near the shock discontinuity, implying fixed energy fractions, ϵ_e and ϵ_B , and thus a constant value of \mathfrak{F} throughout the evolution of the ejecta.

Adopting this evolutionary model, the temporal indices are constrained as follows. The self-similar solution requires that the total energy density scales as $U \propto t^{\alpha_{n_e} + 2\alpha_v}$ where α_{n_e} defines the temporal evolution of the electron density. For a radial dependence of s , we have $\alpha_{n_e} = -s\alpha_r$. Using the scaling for the shock velocity (Equation A2), we then have $U \propto t^{-s\alpha_r + 2(\alpha_r - 1)}$. Similarly, $U_e \propto t^{-s\alpha_r + \alpha_\gamma}$. In a model where ϵ_e and ϵ_B are constant, it follows that $\alpha_{\mathfrak{F}} = 0$ and $U_e \propto U_B \propto U$. This results in the following constraints,

$$\alpha_\gamma = 2(\alpha_r - 1) \tag{9}$$

$$\alpha_B = \frac{(2 - s)}{2}\alpha_r - 1. \tag{10}$$

With the standard assumption that the circumstellar medium is characterized by a wind density profile, $s = 2$, Equation 10 simplifies to $\alpha_B = -1$.

5.2. SSA Model Fit for SN 2003L

Using the SN 2003L multi-frequency radio light-curves and a chosen value of \mathfrak{F}_0 , we fit for the constants C_f and C_τ as well as the temporal index α_r . As discussed in Section 4, ν_m is estimated to be below our radio observing band and we therefore adopt $\nu_{m,0} \approx 1$ GHz. We note that the uncertainty in $\nu_{m,0}$ corresponds to minimal uncertainty in the derived physical parameters as shown by Equations 6 – 8.

Adopting a reference time of $t_0 = 10$ days, we find a best-fit solution ($\chi_r^2 = 7.5$; 105 degrees of freedom) for parameters: $C_f = 7.2 \times 10^{-53}$, $C_\tau = 4.5 \times 10^{38}$, and $\alpha_r = 0.96$. According to Equations 9 – 10, these values imply $\alpha_\gamma = 0.075$ and $\alpha_B = -1.0$. Here, we have used $\mathfrak{F}_0 = 1$ with $\alpha_{\mathfrak{F}} = 0$ and an electron energy index, $p = (-2\beta + 1) = 3.2$, based on the observed optically thin spectral index, $\beta \approx -1.1$ (see Section 2 and Figure 3). As

discussed in the Appendix, we parameterize the sharpness of the ν_a spectral break with $\zeta = [0, 1]$ and find $\zeta \approx 0.5$ for our best-fit solution. The model provides a reasonable fit to the light-curves as seen in Figure 2. We note that the large χ_r^2 is dominated by scintillation, primarily affecting the lower frequency observations.

Better fits can be obtained by relaxing the assumptions of the standard model (hereafter Model 1) as described in Section 5.1. In Model 2, we remove the assumption of a wind density profile and effectively fit for s . For this model we find a best-fit solution ($\chi_r^2 = 5.7$; 104 degrees of freedom) for $C_f = 1.2 \times 10^{-52}$, $C_\tau = 2.5 \times 10^{38}$, $\alpha_r = 0.85$ and $\alpha_B = -0.84$. By Equation 10, this solution implies a shallow CSM density profile of $s = 1.6$. As in the case of Model 1, we have adopted $\mathfrak{F}_0 = 1$, $\alpha_{\mathfrak{F}} = 0$, $p = 3.2$ and $\zeta = 0.5$ for this fit.

A similar fit is obtained by fixing the density profile as $s = 2$ and removing the assumption of constant energy density fractions, ϵ_e and ϵ_B . In this case, Model 3, the constraints given by Equations 9 and 10 do not apply since $\alpha_{\mathfrak{F}}$ is non-zero. By definition, $\mathfrak{F} \propto U_e/U_B$, resulting in the constraint

$$\alpha_{\mathfrak{F}} = -s\alpha_r + \alpha_\gamma - 2\alpha_B \quad (11)$$

which gives $\alpha_{\mathfrak{F}} = -2\alpha_r + \alpha_\gamma - 2\alpha_B$ for $s = 2$. For Model 3, we find a best-fit solution ($\chi_r^2 = 5.7$; 103 degrees of freedom) for $C_f = 1.2 \times 10^{-52}$, $C_\tau = 2.4 \times 10^{38}$, $\alpha_r = 0.78$, $\alpha_B = -1.1$ and $\alpha_\gamma = 0.16$. The implied evolution of \mathfrak{F} is given by $\alpha_{\mathfrak{F}} = 0.88$ with $\epsilon_e \propto t^{0.61}$ and $\epsilon_B \propto t^{-0.27}$. Consistent with Models 1 and 2, $\mathfrak{F}_0 = 1$, $p = 3.2$ and $\zeta = 0.5$ were used for this fit.

A comparison of the best-fit solutions from Models 1 - 3 are shown in Figure 2. It should be noted that Models 2 and 3 produce the same light-curve fit because since they both allow for one extra degree of freedom. While these two models provide a slightly better representation of the SN 2003L data, we adopt Model 1 as our best SSA solution since these assumptions have been shown to be consistent with the full physical model for SN 1993J (Fransson & Björnsson 1998), currently the best-studied radio SN.

5.3. Physical Parameters

Using our solution for Model 1, we find the following values and evolution for B , r and γ_m . The temporal evolution of the magnetic field is $B \approx 4.5(t/t_0)^{-1.0}$ G with an associated radial dependence, $B \propto r^{-1.04}$, similar to that found for the Type IIb SN 1993J ($B \propto r^{-1}$; Fransson & Björnsson 1998). The shock radius is well described by $r \approx 4.3 \times 10^{15}(t/t_0)^{0.96}$ cm

implying a sub-relativistic velocity of $\bar{v} \approx 0.20(t/t_0)^{-0.04} c$. We note that this radial evolution is faster to that of SN 1983N ($r \propto t^{0.86}$; Chevalier 1998) and is within the expected range, $0.67 \leq \alpha_r \leq 1.0$ (Chevalier 1996, 1998). The minimum Lorentz factor of the electrons follows $\gamma_m \approx 8.9(t/t_0)^{-0.08}$ and the implied evolution of ν_m (see Equation A10) is $\nu_m \approx 1.0(t/t_0)^{-1.16}$ GHz which is nearly comparable to the evolution observed for SN 1998bw ($\nu_m \propto t^{-1.0}$; Li & Chevalier 1999) and significantly slower than the decay rate in the adiabatic Sedov-Neumann-Taylor solution ($\nu_m \propto t^{-3}$; Zeldovich & Raizer 2002; Frail, Waxman & Kulkarni 2000).

Using these derived values, additional physical parameters can be computed. The number density of emitting electrons within the circumstellar ejecta, n_e , is thus

$$n_e = \frac{p-2}{p-1} \frac{B_0^2}{8\pi} \frac{\mathfrak{F}_0}{m_e c^2 \gamma_{m,0}} \left(\frac{t}{t_0}\right)^{2\alpha_B - \alpha_\gamma + \alpha_\mathfrak{F}} \text{ cm}^{-3}. \quad (12)$$

Using our above values for \mathfrak{F}_0 , B and $\gamma_{m,0}$, we find $n_e \approx 6.1 \times 10^4 (r/r_0)^{-2.0} \text{ cm}^{-3}$. For $\alpha_r \approx 0.96$ and $s = 2$, the density profile of the ejecta scales steeply as $\rho \propto r^{-27}$.

The associated progenitor mass loss rate is

$$\dot{M} = \frac{8\pi}{\eta} n_e m_p r_0^2 v_w \left(\frac{t}{t_0}\right)^{2\alpha_B - \alpha_\gamma + 2\alpha_r + \alpha_\mathfrak{F}} M_\odot \text{ yr}^{-1} \quad (13)$$

where we have assumed a nucleon-to-proton ratio of 2 and v_w is the velocity of the stellar wind. Assuming a typical wind velocity of $v_w = 1000 \text{ km s}^{-1}$, we find a progenitor mass loss rate of $\dot{M} \approx 7.5 \times 10^{-6} M_\odot \text{ yr}^{-1}$ for SN 2003L. We note that this derived mass loss rate is a factor of ~ 30 larger than that of the Type Ic SN 1998bw and SN 2002ap and yet falls at the low end of values observed for Galactic Wolf-Rayet (WR) stars (Cappa, Goss & van der Hucht 2004), the favored progenitor model for Type Ibc SNe and gamma-ray bursts.

The total ejecta energy, E , is then given as

$$E = \frac{4\pi}{\eta} r_0^3 \frac{\mathfrak{F}_0}{\epsilon_{e,0}} \frac{B_0^2}{8\pi} \left(\frac{t}{t_0}\right)^{2\alpha_B + 3\alpha_r + \alpha_\mathfrak{F} - \alpha_{\epsilon_e}} \text{ erg}. \quad (14)$$

It should be noted that the total energy depends not only on the ratio \mathfrak{F}_0 , but also on assumed value of $\epsilon_{e,0}$. For $\epsilon_{e,0} = 0.1$ (consistent with Li & Chevalier 1999; Berger, Kulkarni & Chevalier 2002) we find an ejecta energy of $E_0 \approx 8.2 \times 10^{47} (t/t_0)^{0.89} \text{ erg}$, just a factor of

two below that of SN 1998bw and 300 times larger than that of SN 2002ap at similar epochs. As discussed by Li & Chevalier (1999), a larger \mathfrak{F}_0 would increase the energy budget further.

For comparison, we derive the physical parameters implied by Models 2 and 3 here. Model 2 shows a slower temporal evolution of radius, $r \approx 5.3 \times 10^{15} (t/t_0)^{0.85}$ cm, and thus a more rapid decline in velocity, $\bar{v} \approx 0.20(t/t_0)^{-0.15}c$. The radio bright ejecta scales as $E \approx 1.0 \times 10^{48}(t/t_0)^{0.88}$ erg and the magnetic field evolves with radius as $B \approx 3.7(r/r_0)^{-0.99}$ G, similar to Model 1. The main difference of Model 2 is that the electron density shows a radial dependence of $n_e \approx 3.7 \times 10^4(r/r_0)^{-1.63}$ cm $^{-3}$, significantly shallower than that associated with a constant circumstellar wind. The density profile of the ejecta is thus given by $\rho \propto r^{-10.7}$ and similar to that found for the Type II SN 1987A ($\rho \propto r^{-9}$; Arnett 1988). This implies an evolution of the mass loss rate, $\dot{M} \approx 6.8 \times 10^{-6}(r/r_0)^{0.37}$ M $_{\odot}$ yr $^{-1}$.

Model 3 shows an even faster deceleration of the ejecta with $\bar{v} \approx 0.20(t/t_0)^{-0.22}c$ and radial evolution of $r \approx 5.3 \times 10^{15}(t/t_0)^{0.78}$ cm. In this case, the energy increases relatively slowly as $E \approx 1.0 \times 10^{48}(t/t_0)^{0.34}$ erg and the magnetic field falls off more steeply as $B \approx 3.7(r/r_0)^{-1.46}$ G. The density profile is fixed at $s = 2$, giving an evolution of $n_e \approx 3.6 \times 10^4(r/r_0)^{-2}$ cm $^{-3}$ and a constant mass loss rate of $\dot{M} \approx 6.8 \times 10^{-6}$ M $_{\odot}$ yr $^{-1}$. We note that Model 3 predicts a relatively shallow ejecta density profile with $\rho \propto r^{-6.25}$. Figure 6 compares the physical parameters predicted by Models 1-3.

6. External Absorption

In the analysis presented above we did not account for the possible effects of external absorption on the observed radio light-curves. For low mass loss rates such as the value we derived through SSA modeling of SN 2003L (Section 5), it has generally been found that free-free absorption (FFA) contributes only minimally to the observed light-curves. Consistent with the SSA model, FFA models assume that the intrinsic radio emission spectrum is due to non-thermal synchrotron processes. The observable signature of FFA is a steepening of the optically thick light-curves at early time (due to contributions from both SSA and FFA processes), as was seen in the case of the Type IIb SN 1993J (Fransson & Björnsson 1998).

6.1. Basic FFA Model

To begin, we fit a basic external absorption model in which the dominant absorption process is assumed to be thermal FFA from a uniform ionized circumstellar medium located external to the ejecta. Following (Weiler *et al.* 1986), this FFA dominated model is given

by

$$f_\nu(t) = K_1 \left(\frac{\nu}{5 \text{ GHz}} \right)^\beta \left(\frac{t}{1 \text{ day}} \right)^{\alpha_f} e^{-\tau_\nu} \text{ mJy}, \quad (15)$$

with

$$\tau_\nu(t) = K_2 \left(\frac{\nu}{5 \text{ GHz}} \right)^{-2.1} \left(\frac{t}{1 \text{ day}} \right)^{\alpha_\tau}. \quad (16)$$

where α_f and α_τ describe the temporal evolution of the flux density and optical depth, respectively; K_1 and K_2 are normalization constants and β is the optically thin spectral index.

As shown in Figure 7, the basic FFA model fit (thin solid line) provides a poor match to the data, underestimating the slow turn-on of the radio emission with $\chi_r^2 \approx 14.0$ (two times worse than the SSA model fit, § 5). The fitted parameter values are $K_1 \approx 597$, $\beta \approx -1.0$, $\alpha_f \approx -0.97$, $K_2 \approx 1710$ and $\alpha_\tau \approx -1.5$.

According to this FFA dominated model, we estimate the predicted mass loss rate of the progenitor star using Equation 17 of Weiler, Panagia & Montes (2001). We find a high mass loss rate of $\dot{M} \approx 1.4 \times 10^{-2} M_\odot \text{ yr}^{-1}$ (for $v_w = 1000 \text{ km s}^{-1}$). This value is three orders of magnitude above the typical mass loss rate for Galactic Wolf-Rayet stars, which show $\dot{M} \approx 10^{-5} M_\odot \text{ yr}^{-1}$ with $v_w \approx 1000$ to 2000 km s^{-1} (Cappa, Goss & van der Hucht 2004).

6.2. Complex FFA Model

Better light-curve fits are obtained by applying the complex FFA model of Weiler, Panagia & Montes (2001) which includes multiple external absorption processes, each characterized by the distribution of absorbing material (uniform vs clumpy) and the location of the material with respect to the radiating electrons (within the CSM vs distant). We note that this FFA model also allows for both internal SSA and FFA components to contribute to the shape of the observed radio light-curves.

Applying this model to the SN 2003L radio light-curves, we find that the two dominant absorption processes are internal SSA and external FFA due to a clumpy CSM. In the notation of Weiler, Panagia & Montes (2001) this corresponds to $K_1 \approx 2.80 \times 10^3$, $\alpha \approx -1.11$, $\beta \approx -1.24$, $K_3 \approx 7.66 \times 10^4$, $\delta' \approx -2.15$, $K_5 \approx 1.28 \times 10^3$, $\delta'' \approx -1.60$, with all other parameters effectively insignificant. As shown in Figure 7, the complex FFA solution (thick solid line) provides an reasonable fit to the data with $\chi_r^2 = 4.5$ for 96 dof.

To estimate the physical parameters of the SN in this model we remove the external absorption due to the clumpy CSM component leaving only the intrinsic synchrotron self-absorbed spectrum. As shown in Figure 7, at $t \approx 2$ days the peak flux density is $f_p \approx 102.1$ mJy at $\nu_p \approx 22.5$ GHz and $\beta \approx -1.1$. For these values, Equations 2 and 3 give an equipartition radius of $r_{\text{ep}} \approx 5.7 \times 10^{16}$ cm, an expansion velocity of $\bar{v}_{\text{ep}} \approx 14c$, and an ejecta energy of $E_{\text{ep}} \approx 7.0 \times 10^{48}$ erg. With this velocity, the ejecta radius would be $r \approx 2.4 \times 10^{18}$ cm at $t \approx 65$ days, in violation of the VLBA limit of $r \leq 9.1 \times 10^{17}$ cm. To match the observed VLBA limit, we relax the assumption of equipartition, but this results in a steep increase in the total ejecta energy by a factor of ~ 300 , giving $E \approx 3 \times 10^{51}$. Moreover, we note that the model is parameterized for the case of non-relativistic ejecta speeds and is therefore inconsistent with the implied relativistic velocity. A consistent, non-relativistic solution to the Weiler, Panagia & Montes (2001) model could not be found for the case of SN 2003L.

7. Modeling the X-ray emission

X-ray emission in supernovae can be produced by three processes (Fransson, Lundqvist & Chevalier 1996): (1) non-thermal synchrotron emission from radiating electrons, (2) thermal (free-free) bremsstrahlung emission from material in the circumstellar shock and/or the ejecta reverse shock, and (3) inverse Compton scattering of photospheric photons by relativistic electrons. We examine each of these scenarios in the context of the bright X-ray emission of SN 2003L.

7.1. Synchrotron Emission

Extrapolating the (optically thin) synchrotron emission at $t \approx 40$ days from the radio to the X-ray band as $f_\nu \propto \nu^\beta$ with $\beta \approx -1.1$, we find that the synchrotron emission under-predicts the observed X-ray flux by a factor of ~ 50 . The discrepancy is significantly larger when a synchrotron cooling break, ν_c , is included, beyond which the spectrum steepens by $\Delta\beta = -0.5$ (see the Appendix). Using Equation A16 together with the magnetic field evolution derived in Section 5, the cooling frequency at $t \approx 40$ days is $\nu_c \approx 1.1 \times 10^{11}$ Hz. Including this synchrotron break and extrapolating from ν_c to $\nu_{\text{X-ray}}$ as $f_\nu \propto \nu^{-1.6}$, the synchrotron emission in the X-ray grossly under-predicts the observed flux by 5 orders of magnitude. We also note that the flat spectrum, $\beta \approx -0.5$, of the observed X-rays is inconsistent with the steep synchrotron spectral index observed in the radio bands, $\beta \approx -1.1$. We therefore conclude that the X-ray emission is not due to synchrotron processes.

7.2. Thermal Bremsstrahlung Emission

In a scenario dominated by thermal bremsstrahlung processes, the X-ray emission is produced by the forward shock plowing into circumstellar material and/or the reverse shock heating of the ejecta. In this case, the strength of the X-ray emission depends of the density of the emitting material. The shocked material then cools by free-free emission processes. For an $n_e \propto r^{-2}$ wind density profile, free-free luminosity from the forward or reverse shock is generalized (Chevalier & Fransson 2003; Sutaria *et al.* 2003) roughly by

$$L_X \approx 7.5 \times 10^{34} C_L \left(\frac{\dot{M}}{10^{-5} M_\odot \text{ yr}^{-1}} \right)^2 \left(\frac{1000 \text{ km/s}}{v_w} \right)^2 \left(\frac{t}{40 \text{ days}} \right)^{-1} \text{ erg s}^{-1} \quad (17)$$

where C_L is a constant such that $C_L = C_{\text{FS}} = 1$ for the forward shock and $C_L = C_{\text{RS}} = (n-3)(n-4)^2/(4n-8)$ for the reverse shock. For SSA Model 1 (Section 5), we find $\alpha_r \approx 0.96$ and thus $n \approx 27$ and $C_{\text{RS}} \approx 127$. Using the mass loss rate derived from Model 1, the *combined* free-free luminosity from the forward and reverse shocks is therefore $L_{X,\text{FS+RS}} \approx 5.4 \times 10^{36} \text{ erg s}^{-1}$, and a factor $\sim 10^3$ fainter than that observed. On the other hand, if we assume the X-ray emission *must* be dominated by free-free processes, then this implies a mass loss rate of $2.7 \times 10^{-4} M_\odot \text{ yr}^{-1}$ ($v_w = 1000 \text{ km s}^{-1}$), which is inconsistent with both the rate predicted by radio SSA models as well as that associated with FFA modeling (Section 6).

7.3. Inverse Compton Cooling

X-ray emission from supernovae can also be produced by inverse Compton (IC) cooling of the relativistic electrons by the optical photons as was claimed to be important for the X-ray emission of SN 2002ap (Björnsson & Fransson 2004). In this scenario, the ratio of energy densities in magnetic fields, U_B , and photons, U_{ph} , is given roughly by

$$\frac{f_{\text{radio}}}{f_{\text{X-ray}}} \approx \frac{U_B}{U_{\text{ph}}} \quad (18)$$

where $f_{\text{radio}} \equiv \nu f_\nu$ is the optically thin synchrotron flux in the radio band and f_X is the corresponding X-ray flux. At $t \approx 40$ days, the observed radio flux was $f_{\text{radio}} \approx 6.7 \times 10^{-16} \text{ erg cm}^{-2} \text{ s}^{-1}$ and the X-ray flux was $f_{\text{X-ray}} \approx 9.2 \times 10^{-15} \text{ erg cm}^{-2} \text{ s}^{-1}$, giving a ratio of $f_{\text{radio}}/f_{\text{X-ray}} \approx 0.074$.

Assuming the timescale for Compton cooling is comparable to the epoch *Chandra* observations, $t_{\text{comp}} \approx 40$ days, and using Equations (14–18) of Björnsson & Fransson (2004), we are able to roughly match the observed X-ray luminosity. Since we see no evidence for IC cooling affects within our radio light-curves, we place a lower limit of $\nu_{\text{IC}} \geq 22$ GHz. This implies constraints on the magnetic field and shock velocity of $B \geq 0.4$ G and $v \geq 0.09c$, consistent with the values predicted from SSA radio analyses (§ 5). The corresponding limit on the energy density in magnetic fields is thus $U_B \gtrsim 0.0048$ erg cm⁻³ and is therefore consistent with the value found through SSA Model 1 (§ 5). We note that in these estimates, a bolometric luminosity of $L_{\text{bol},42} \approx 1.5$ has been very roughly estimated based on fitting the SN 2003L optical light-curve (Soderberg *et al.* 2004).

While inverse Compton cooling appears to be a feasible process to produce the luminous X-ray emission of SN 2003L, it predicts a steep spectral index, $\beta_{\text{X-ray}} \approx \beta_{\text{radio}} \approx -1.1$, which is inconsistent with the observed value of $\beta \approx -0.5$ ($2 - \sigma$). We note, however, that the poor photon statistics may be responsible for this discrepancy.

8. Discussion and Conclusions

As the first Type Ibc supernova with a radio and X-ray luminosity within an order of magnitude of SN 1998bw, SN 2003L is clearly an unusual event. Here, we summarize our findings. Both SSA and FFA models (Sections 5 and 6) show that the energy of the ejecta is $\gtrsim 10^{48}$ erg and nearly comparable to that of SN 1998bw at a similar epoch. In Case 1 the equipartition and SSA analyses predict a sub-relativistic velocity, $\bar{v} \approx 0.2c$, and a relatively low mass loss rate, $\dot{M} \approx 7.5 \times 10^{-6} M_{\odot} \text{ yr}^{-1}$ which are roughly consistent with a scenario where inverse Compton scattering produces the observed X-ray emission. In Case 2, the complex FFA models reproduce the observed radio light-curves well, yet they imply a highly relativistic ejecta speed, $\bar{v} \approx 14c$, or a huge energy output of $E \geq 10^{51}$ erg, as well as a high mass loss rate of $\dot{M} \approx 10^{-2} M_{\odot} \text{ yr}^{-1}$ which over-predicts the observed X-ray emission assuming a thermal bremsstrahlung emission model.

Our VLBA observation at $t \approx 65$ days implies an ejecta size which is inconsistent with the extreme velocities required by the complex FFA model in Case 2. Only by deviating far from equipartition and significantly increasing the total energy of the ejecta can this inconsistency be resolved. Moreover, the predicted mass loss rate is at least two orders of magnitude above the observed rates from Wolf-Rayet stars. In conclusion, we find Case 2 to be infeasible and we therefore adopt Case 1 the most likely scenario. We note that Case 1 predicts a mass loss rate comparable to the low end of values observed for local Wolf-Rayet stars.

While similar to SN 1998bw in radio luminosity and ejecta energy, a main distinguishing characteristic between SN 2003L and SN 1998bw is their shock velocity: while the radio ejecta of SN 1998bw attained mildly-relativistic speeds, that of SN 2003L was clearly sub-relativistic as shown in Section 5. This discrepancy is echoed by optical spectroscopy which showed photospheric velocities in excess of $3 \times 10^4 \text{ km s}^{-1}$ for SN 1998bw (Patat *et al.* 2001) and 10^4 km s^{-1} for SN 2003L (Valenti *et al.* 2003; Matheson *et al.* 2003; Soderberg *et al.* 2004). Therefore, we see that for SN 1998bw, mildly-relativistic ejecta was coupled with bright radio emission, while for SN 2003L the emission is bright *despite* the modest ejecta velocities. The question is thus, why is the radio ejecta of SN 2003L especially luminous and energetic?

One hypothesis considers the distribution of kinetic energy according to ejecta velocity. SN 1998bw is a clear case where a significant fraction of the explosion energy has been deposited into mildly-relativistic material. For SN 2003L, however, the bulk of the energy is coupled to sub-relativistic ejecta. Tan, Matzner & McKee (2001) have shown that in some cases, high velocity ejecta can be produced from a whip effect racing down the ejecta. The observed diversity in the coupling between velocity and energy could therefore be intrinsic to the SN Ibc population. A similar situation is observed for gamma-ray bursts which partition their energy into ultra-relativistic emission (γ -rays) and mildly-relativistic afterglow emission (X-rays, optical, radio) by variable fractions.

Through our ongoing radio surveys of local SNe Ibc and cosmological gamma-ray bursts, we continue to map out the energetics of these explosions. Our goal is to understand the link between Type Ibc supernovae and GRBs by studying properties of the explosion (ejecta velocity and kinetic energy) in addition to those of the progenitor star (CSM density profile and evolutionary mass loss rate). Through these further studies, we aim to shed light on the illusive bridge between these two classes of cosmic explosions.

We are indebted to Barry Clark for his generous scheduling of the VLA for this project, and to Jim Ulvestad for enabling the VLBA observations. The authors thank Re'em Sari, Claes Fransson, Eli Waxman, Dick Sramek and Michael Rupen for useful discussions. Caltech SN research is supported by NSF and NASA grants. AMS acknowledges support by the National Radio Astronomy Observatory Graduate Summer Student Research Assistantship program. Research by EB is supported by NASA through Hubble Fellowship grant HST-HF-01171.01 awarded by the Space Telescope Science Institute, which is operated by the Association of Universities for Research in Astronomy, Inc., for NASA, under contract NAS 5-26555. RAC thanks NSF grant AST-0307366.

Appendix

A. The Synchrotron Self-Absorption Model

Here we describe the SSA model prescription applied in Section 5. The model was adapted from the formalism of (Frail, Waxman & Kulkarni 2000), designed to describe gamma-ray burst radio emission following the transition to sub-relativistic, adiabatic expansion. We replace the assumption of Sedov-Neumann-Taylor (SNT) dynamics (Zeldovich & Raizer 2002) with a general parameterization of the shock evolution. This substitution enables us to study the early supernova synchrotron emission, while the ejecta is in the free-expansion phase. We note that by adopting the scalings given by the SNT dynamics into our generalized equations, the formalism of Frail, Waxman & Kulkarni (2000) is fully recovered.

A.1. Physical Assumptions

To first order, we assume that the supernova ejecta is undergoing spherical, homologous expansion at sub-relativistic velocity, v . At any time, t , the observed synchrotron emission originates from a thin shell of radiating electrons with radius, r , and thickness, r/η (with $\eta \approx 10$). The electrons are accelerated into a power-law energy distribution, $N(\gamma) \propto \gamma^{-p}$, above a minimum Lorentz factor, γ_m . We adopt the standard assumption that the energy density of the ejecta is partitioned between the fraction in relativistic electrons, ϵ_e , and the fraction in magnetic fields, ϵ_B . For simplicity, we denote the ratio of these energies as $\mathfrak{F} \equiv \epsilon_e/\epsilon_B$ and further assume that it evolves as $\mathfrak{F} \propto t^{\alpha_{\mathfrak{F}}}$.

The temporal evolution of the radius, velocity, minimum Lorentz factor and magnetic field are then parameterized as

$$r = r_0 \left(\frac{t}{t_0} \right)^{\alpha_r} \tag{A1}$$

$$v = v_0 \left(\frac{t}{t_0} \right)^{\alpha_v} \tag{A2}$$

$$\gamma_m = \gamma_{m,0} \left(\frac{t}{t_0} \right)^{\alpha_{\gamma}} \tag{A3}$$

$$B = B_0 \left(\frac{t}{t_0} \right)^{\alpha_B} \tag{A4}$$

where the subscript 0 corresponds to the parameter values at an (arbitrary) reference time, t_0 . Here, the indices α_r , α_γ , α_B and $\alpha_\mathfrak{F}$ are determined by the hydrodynamic evolution of the ejecta, and are constrained according to the assumed evolutionary model (see Section 5.1).

A.2. Emission Spectrum

In characterizing the synchrotron emission spectrum, we use the standard formalism of Rybicki & Lightman (1979). Within this framework, the synchrotron power per unit frequency emitted by a single electron is given by

$$P(\nu, \gamma) = \frac{e^3 B}{m_e c^2} F\left(\frac{\nu}{\nu_{\text{crit}}(B, \gamma)}\right) \quad (\text{A5})$$

where γ , e and m_e are the Lorentz factor, charge and mass of the electron, respectively. The critical frequency, ν_{crit} , is defined as

$$\nu_{\text{crit}} \equiv \gamma^2 \left(\frac{eB}{2\pi m_e c}\right) \quad (\text{A6})$$

(Rybicki & Lightman 1979). Adopting the notation $x \equiv (2/3)(\nu/\nu_{\text{crit}})$, the function $F(x)$ describes the total synchrotron power spectrum.

$$F(x) \equiv x \int_x^\infty K_{5/3}(\xi) d\xi \quad (\text{A7})$$

where $K_{5/3}$ is the modified Bessel function of 2/3 order (Rybicki & Lightman 1979). This function peaks at $x = 0.29$ and decays rapidly for $x > 1$.

Applying the temporal scalings for r , β , B and γ_m (Equations A1 - A4), the flux density from a uniform shell of radiating electrons is then given by

$$f_\nu(t) = C_f \left(\frac{t}{t_0}\right)^{(4\alpha_r - \alpha_B)/2} [(1 - e^{-\tau_\nu^\zeta(t)})]^{1/\zeta} \nu^{5/2} F_3(x) F_2^{-1}(x) \text{ erg/s/Hz/cm}^2 \quad (\text{A8})$$

where the optical depth, $\tau_\nu(t)$, is defined

$$\tau_\nu(t) = C_\tau \left(\frac{t}{t_0}\right)^{(p-2)\alpha_\gamma + (3+p/2)\alpha_B + \alpha_r + \alpha_\mathfrak{F}} \nu^{-(p+4)/2} F_2(x) \quad (\text{A9})$$

and $\zeta = [0, 1]$ parameterizes the sharpness of the spectral break between optically thick and thin regimes. We adopt $\nu_m \equiv \nu_{\text{crit}}(\gamma = \gamma_m)$ as the characteristic synchrotron frequency,

$$\nu_m(t) = \nu_{m,0} \left(\frac{t}{t_0} \right)^{2\alpha_\gamma + \alpha_B} \text{ Hz}, \quad (\text{A10})$$

and for $x = (2/3)(\nu/\nu_m(t))$, the functions, $F_2(x)$ and $F_3(x)$, are defined

$$F_2(x) \equiv \sqrt{3} \int_0^x F(y) y^{(p-2)/2} dy, \quad F_3(x) \equiv \sqrt{3} \int_0^x F(y) y^{(p-3)/2} dy \quad (\text{A11})$$

where y is a simple integration variable representing the range $y = [0, x]$. The temporal dependencies of $F_2(x)$ and $F_3(x)$ can be computed numerically. For $\nu \ll \nu_m$, we find the following scalings

$$F_2(x) \propto t^{0.49(p+0.73)}, \quad F_3(x) \propto t^{0.47(p-0.14)} \quad (\text{A12})$$

and for $\nu \gg \nu_m$, neither function evolves. Therefore, using equations A8 through A12, the model flux density at any time is strictly determined by three parameters: C_f , C_τ and $\nu_{m,0}$:

$$C_f \equiv \frac{2\pi}{2+p} m_e \left(\frac{r_0}{d} \right)^2 \left(\frac{2\pi m_e c}{e B_0} \right)^{1/2} \quad (\text{A13})$$

$$C_\tau \equiv \frac{(p+2)(p-2)}{4\pi\eta} \gamma_{m,0}^{(p-1)} \left(\frac{B_0^2}{8\pi} \mathfrak{F}_0 \right) \left(\frac{e^3 B_0 r_0}{m_e^3 c^4 \gamma_{m,0}} \right) \left(\frac{e B_0}{2\pi m_e c} \right)^{p/2} \quad (\text{A14})$$

$$\nu_{m,0} \equiv \frac{1}{2\pi} \gamma_{m,0}^2 \frac{e B_0}{m_e c} \quad (\text{A15})$$

where d is the distance to the source and \mathfrak{F}_0 is the value of \mathfrak{F} at t_0 . Equations A13 - A15 above show that C_f , C_τ and $\nu_{m,0}$ are in turn determined by four physical parameters: B_0 , r_0 , $\gamma_{m,0}$ and \mathfrak{F}_0 .

A.3. Temporal and Spectral Evolution

We use the above formalism to determine the spectral evolution of the synchrotron emission for a given ordering of the synchrotron break frequencies, ν_a and ν_m . Here, we

define the self-absorption frequency, ν_a , as the frequency at which the optical depth is unity: $\tau_{\nu_a} \equiv \tau(\nu = \nu_a) = 1$.

For completeness, we give the temporal and spectral evolution for higher frequencies near the synchrotron cooling frequency, ν_c , defined as the the frequency above which electrons cool efficiently. This frequency is given by

$$\nu_c = \frac{18\pi m_e c e}{t^2 \sigma_T^2 B^3} \text{ Hz} \quad (\text{A16})$$

and is typically located between the radio and optical observing bands during the first few years after the supernova explosion.

A.3.1. Case 1: $\nu_a \ll \nu_m$

In Case 1, the self-absorption frequency is well below the characteristic synchrotron frequency, $\nu_a \ll \nu_m$. In this scenario, the spectrum peaks at $\nu_p \approx \nu_m$. It can be shown that the temporal scalings associated with the peak are then given by,

$$\nu_p \approx \nu_m \propto t^{2\alpha_\gamma + \alpha_B}, \quad f_{\nu_p} \approx f_{\nu_m} \propto t^{3\alpha_r + 3\alpha_B - \alpha_\gamma + \alpha_\delta} \quad (\text{A17})$$

Here, $\nu_a \ll \nu_m$ so the evolution of ν_a and f_{ν_a} depend on the temporal scaling of $F_2(x)$ (Equation A12). We find

$$\nu_a \propto t^{(2(p-136)\alpha_\gamma + (p+264)\alpha_B + 100\alpha_r + 100\alpha_\delta)/(p+164)}, \quad f_{\nu_a} \propto t^{(9\alpha_r + 8\alpha_B - 5\alpha_\gamma + \alpha_{\nu_a} + 3\alpha_\delta)/3} \quad (\text{A18})$$

where, for simplicity, we use α_{ν_a} to denote the temporal dependence of ν_a . For all frequencies, the temporal and frequency dependence of f_ν is then generalized by

$$f_\nu \propto \begin{cases} \nu^2 t^{(9\alpha_r + 8\alpha_B - 5\alpha_\gamma - 5\alpha_{\nu_a} + 3\alpha_\delta)/3} & \nu < \nu_a \\ \nu^{1/3} t^{(9\alpha_r + 8\alpha_B - 5\alpha_\gamma + 3\alpha_\delta)/3} & \nu_a < \nu < \nu_m \\ \nu^{-(p-1)/2} t^{(6\alpha_r + (5+p)\alpha_B + 2(p-2)\alpha_\gamma + 2\alpha_\delta)/2} & \nu_m < \nu < \nu_c \\ \nu^{-p/2} t^{(6\alpha_r + (8-5p)\alpha_B + 2(p-2)\alpha_\gamma + 2\alpha_\delta - 4p+2)/2} & \nu_c < \nu \end{cases} \quad (\text{A19})$$

where the temporal scalings associated with the synchrotron cooling frequency are

$$\nu_c \propto t^{-3\alpha_B-2}, \quad f_{\nu_c} \propto t^{3\alpha_r+(4-p)\alpha_B+(p-2)\alpha_\gamma+\alpha_\delta-p+1}. \quad (\text{A20})$$

A.3.2. *Case 2: $\nu_m \ll \nu_a$*

In Case 2, the characteristic synchrotron frequency is below the self-absorption frequency, $\nu_m \ll \nu_a$. In this case, the spectral peak occurs at $\nu_p \approx \nu_a$. Since $F_2(x)$ is constant for $\nu \gg \nu_m$, the scalings simplify to

$$\nu_p \approx \nu_a \propto t^{(2(p-2)\alpha_\gamma+2(3+p/2)\alpha_B+2\alpha_r+2\alpha_\delta)/(p+4)}, \quad f_{\nu_p} \approx f_{\nu_a} \propto t^{(4\alpha_r-\alpha_B+5\alpha_{\nu_a})/2}. \quad (\text{A21})$$

In this scenario, the evolution of ν_m is given by Equation A10 while F_{ν_m} scales as

$$f_{\nu_m} \propto t^{2\alpha_r+2\alpha_B+5\alpha_\gamma}. \quad (\text{A22})$$

For all frequencies, the temporal and frequency dependence of f_ν is then generalized by

$$f_\nu \propto \begin{cases} \nu^2 t^{2\alpha_r+\alpha_\gamma} & \nu < \nu_m \\ \nu^{1/3} t^{(4\alpha_r-\alpha_B)/2} & \nu_m < \nu < \nu_a \\ \nu^{-(p-1)/2} t^{(4\alpha_r-\alpha_B+(4+p)\alpha_{\nu_a})/2} & \nu_a < \nu < \nu_c \\ \nu^{-p/2} t^{(2\alpha_r+(1-3p)\alpha_B+(2+p/2)\alpha_{\nu_a}-2p+1)} & \nu_c < \nu \end{cases} \quad (\text{A23})$$

where the temporal scalings associated with the synchrotron cooling frequency are

$$\nu_c \propto t^{-3\alpha_B-2}, \quad f_{\nu_c} \propto t^{(4\alpha_r+(3-3p)\alpha_B+(4+p)\alpha_{\nu_a}-2p+2)/2}. \quad (\text{A24})$$

REFERENCES

- Arnett, W. D. 1988, ApJ, 331, 377.
- Berger, E., Kulkarni, S. R., and Chevalier, R. A. 2002, ApJ, 577, L5.
- Berger, E., Kulkarni, S. R., Frail, D. A., and Soderberg, A. M. 2003, ApJ, 599, 408.

- Björnsson, C. and Fransson, C. 2004, ApJ, 605, 823.
- Bloom, J. S. *et al.* 1999, Nature, 401, 453.
- Bloom, J. S. *et al.* 2002, ApJ, 572, L45.
- Boles, T. 2003, IAU Circ., 8048, 1.
- Cappa, C., Goss, W. M., and van der Hucht, K. A. 2004, AJ, 127, 2885.
- Chevalier, R. A. 1996, in ASP Conf. Ser. 93: Radio Emission from the Stars and the Sun, 125.
- Chevalier, R. A. 1998, ApJ, 499, 810.
- Chevalier, R. A. and Fransson, C. 2003, in Supernovae and Gamma-ray Bursters, ed. K. W. Weiler (Berlin: Springer), 171.
- Dickey, J. M. and Lockman, F. J. 1990, ARA&A, 28, 215.
- Frail, D. A., Waxman, E., and Kulkarni, S. R. 2000, ApJ, 537, 191.
- Fransson, C. and Björnsson, C. 1998, ApJ, 509, 861.
- Fransson, C., Lundqvist, P., and Chevalier, R. A. 1996, ApJ, 461, 993.
- Galama, T. J. *et al.* 1998, Nature, 395, 670.
- Kellermann, K. I. and Pauliny-Toth, I. I. K. 1981, ARA&A, 19, 373.
- Kulkarni, S. and Fox, D. W. 2003, IAU Circ., 8073, 2.
- Kulkarni, S. R. *et al.* 1998, Nature, 395, 663.
- Li, Z. and Chevalier, R. A. 1999, ApJ, 526, 716.
- Matheson, T., Challis, P., Kirshner, R. P., and Garnavich, P. M. 2003, GRB Circular Network, 1846, 1.
- Patat, F. *et al.* 2001, ApJ, 555, 900.
- Pian, E. *et al.* 2000, ApJ, 536, 778.
- Predehl, P. and Schmitt, J. H. M. M. 1995, A&A, 293, 889.
- Price, P. A. *et al.* 2003, ApJ, 584, 931.

- Rybicki, G. B. and Lightman, A. P. 1979, *Radiative Processes in Astrophysics*, (New York: Wiley).
- Schlegel, D. J., Finkbeiner, D. P., and Davis, M. 1998, *ApJ*, 500, 525.
- Soderberg, A. M., Kulkarni, S. R., Gal-Yam, A., Fox, D. B., and Cenko, S. B. 2004, in prep.
- Stanek, K. Z. *et al.* 2003, *ApJ*, 591, L17.
- Sutaria, F. K., Chandra, P., Bhatnagar, S., and Ray, A. 2003, *A&A*, 397, 1011.
- Tan, J. C., Matzner, C. D., and McKee, C. F. 2001, *ApJ*, 551, 946.
- Valenti, S., Cappellaro, E., Danese, S., Di Pede, G., Navasardyan, H., Pastorello, A., Benetti, S., and Turatto, M. 2003, *IAU Circ.*, 8057, 2.
- Weiler, K. W., Panagia, N., and Montes, M. J. 2001, *ApJ*, 562, 670.
- Weiler, K. W., Sramek, R. A., Panagia, N., van der Hulst, J. M., and Salvati, M. 1986, *ApJ*, 301, 790.
- Zel'dovich, Y. B. and Raizer, Y. P. 2002, *Physics of Shock Waves and High Temperature Hydrodynamic Phenomena*, (Minola, NY: Dover).

Table 1. VLA radio flux density measurements of SN 2003L

Date (UT)	Δt (days)	$F_{4.9 \text{ GHz}} \pm \sigma$ (μJy)	$F_{8.5 \text{ GHz}} \pm \sigma$ (μJy)	$F_{15.0 \text{ GHz}} \pm \sigma$ (μJy)	$F_{22.5 \text{ GHz}} \pm \sigma$ (μJy)	Array Config.
2003 Jan 26.2	25.2	—	743±39	—	—	DnC
2003 Jan 28.3	27.3	—	810±63	—	3179±85	DnC
2003 Jan 29.3	28.3	—	848±65	—	3119±86	DnC
2003 Jan 30.4	29.4	—	966±60	—	3122±75	DnC
2003 Jan 31.3	30.3	—	1051±62	—	3080±86	DnC
2003 Feb 1.2	31.2	—	947±52	—	3252±70	DnC
2003 Feb 2.3	32.3	—	883±53	—	2973±99	DnC
2003 Feb 3.3	33.3	—	—	2287±121	—	DnC
2003 Feb 6.3	36.3	—	1147±47	—	—	DnC
2003 Feb 8.3	38.3	—	1211±39	—	—	D
2003 Feb 11.6	41.6	—	1483±76	2686±156	2956±96	D
2003 Feb 14.5	44.5	—	1448±62	2753±153	2684±124	D
2003 Feb 16.4	46.4	—	1413±55	2719±144	—	D
2003 Feb 18.4	48.4	—	1546±45	—	—	D
2003 Feb 22.3	52.3	—	—	3014±137	2714±68	D
2003 Feb 23.3	53.3	—	1854±41	—	—	D
2003 Feb 25.3	55.3	—	1969±53	2799±149	2838±99	D
2003 Feb 26.3	56.3	—	—	2865±131	—	D
2003 Mar 2.3	60.3	—	2283±51	2924±132	—	D
2003 Mar 7.3	65.3	848±64 ^a	—	—	2263±73	D
2003 Mar 8.4	66.4	—	2351±47	2857±123	2486±66	D
2003 Mar 10.3	68.3	—	2081±52	2966±115	—	D
2003 Mar 14.4	72.4	—	2527±52	2901±150	2422±70	D
2003 Mar 17.4	75.4	—	2673±57	3055±173	—	D
2003 Mar 20.3	78.3	—	2422±61	—	2130±223	D
2003 Mar 23.3	81.3	—	2500±43	2664±118	—	D
2003 Mar 27.4	85.4	—	2776±51	—	1833±100	D
2003 Apr 1.2	90.2	—	2551±54	—	—	D
2003 Apr 2.1	91.1	—	—	—	1819±141	D

Table 1—Continued

Date (UT)	Δt (days)	$F_{4.9 \text{ GHz}} \pm \sigma$ (μJy)	$F_{8.5 \text{ GHz}} \pm \sigma$ (μJy)	$F_{15.0 \text{ GHz}} \pm \sigma$ (μJy)	$F_{22.5 \text{ GHz}} \pm \sigma$ (μJy)	Array Config.
2003 Apr 10.4	99.4	—	—	2581±320	—	D
2003 Apr 30.0	119.0	—	2532±75	—	1078±173	D
2003 May 3.1	122.1	—	2534±80	—	1327±114	D
2003 May 16.3	135.3	—	2455±96	1925±282	1146±165	D
2003 May 28.1	147.0	1989±41	2200±47	1452±235	941±161	D
2003 Jun 4.0	154.0	2410±114	2151±77	—	—	A
2003 Jun 17.1	167.1	2555±83	2210±68	1279±226	—	A
2003 Jul 1.1	181.1	—	2262±63	—	—	A
2003 Jul 9.0	189.0	2485±90	2075±61	1135±125	—	A
2003 Jul 24.0	204.0	2380±81	2048±66	1177±166	—	A
2003 Aug 11.9	222.9	—	—	—	670±148	A
2003 Aug 15.8	226.8	2346±84	1646±74	824±237	—	A
2003 Sep 15.7	257.7	2177±87	1151±53	768±165	—	A
2003 Oct 6.7	278.6	2140±40	1244±58	—	—	BnA
2003 Oct 11.7	283.7	2177±79	1176±45	612±122	—	BnA
2003 Oct 27.7	299.7	1937±70	1200±42	520±124	—	B
2003 Nov 1.7	304.7	—	1115±55	—	—	B
2003 Nov 14.6	317.6	1713±73	1075±52	—	—	B
2003 Nov 25.5	328.5	1689±67	981±49	148±148	—	B
2003 Dec 6.6	339.6	1980±69	961±42	506±149	—	B
2004 Jan 26.4	390.4	—	714±38	—	—	B
2004 Feb 8.3	403.3	—	863±42	—	—	CnB
2004 Mar 6.4	430.4	1281±42	—	—	—	C
2004 Mar 20.2	444.2	—	668±30	—	—	C
2004 Apr 21.0	476.0	—	—	125±137	—	C
2004 May 21.0	506.0	—	—	—	280±53	D
2004 Jul 27.0	573.0	—	592±48	—	—	D

^aVLBA observation

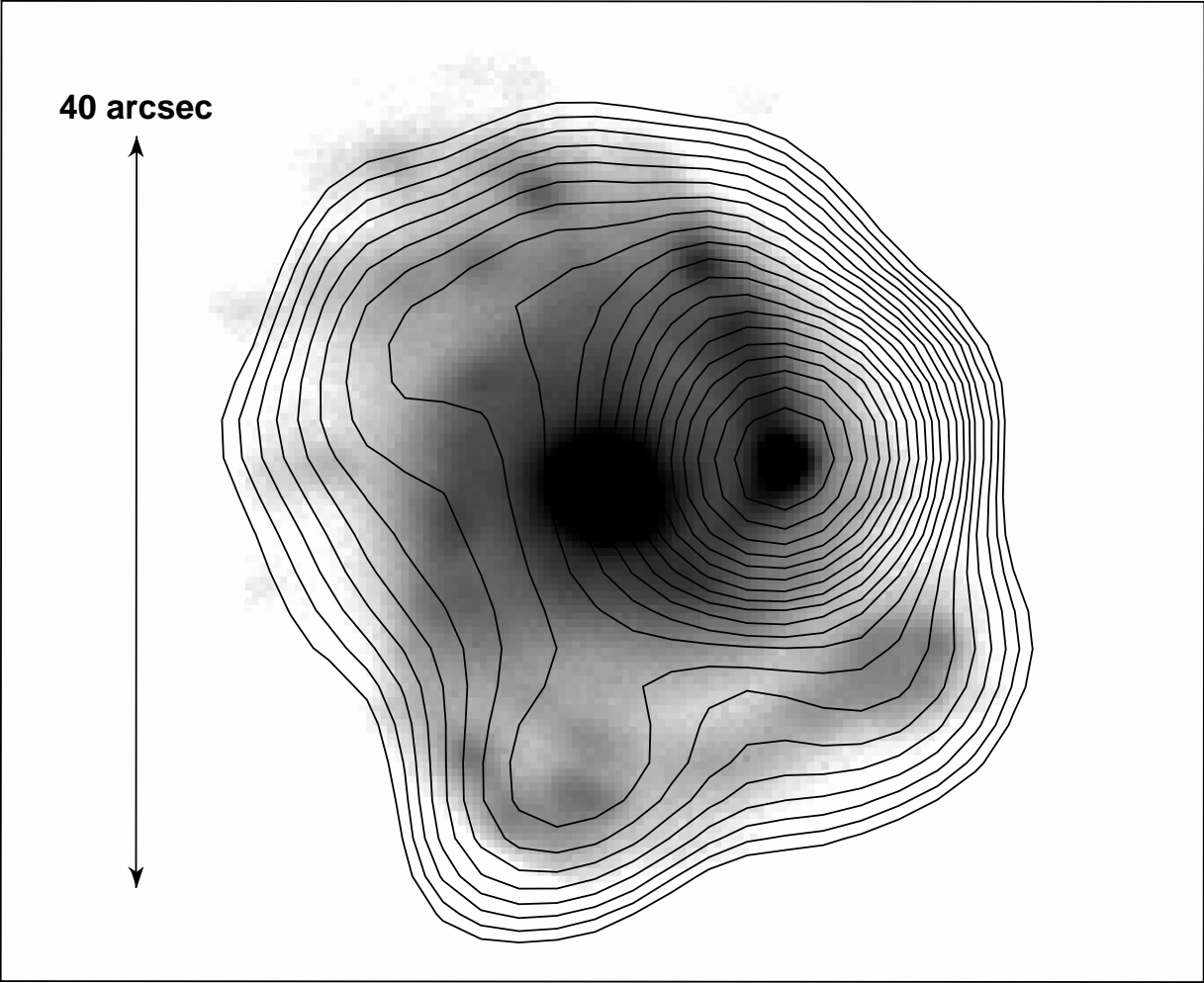


Fig. 1.— Optical and radio emission from SN 2003L at $t \sim 35$ days. A Palomar 60-inch R -band image (greyscale) shows the SN located within a spiral arm of host galaxy NGC 3506. Twenty-five radio (8.5 GHz) map contours are over-plotted from 0.15 mJy (3-sigma) to 4.0 mJy in equally spaced logarithmic intervals. The radio emission peaks at the optical position of SN 2003L and diffuse emission from the host galaxy extends a size of approximately 45 by 45 arcsec.

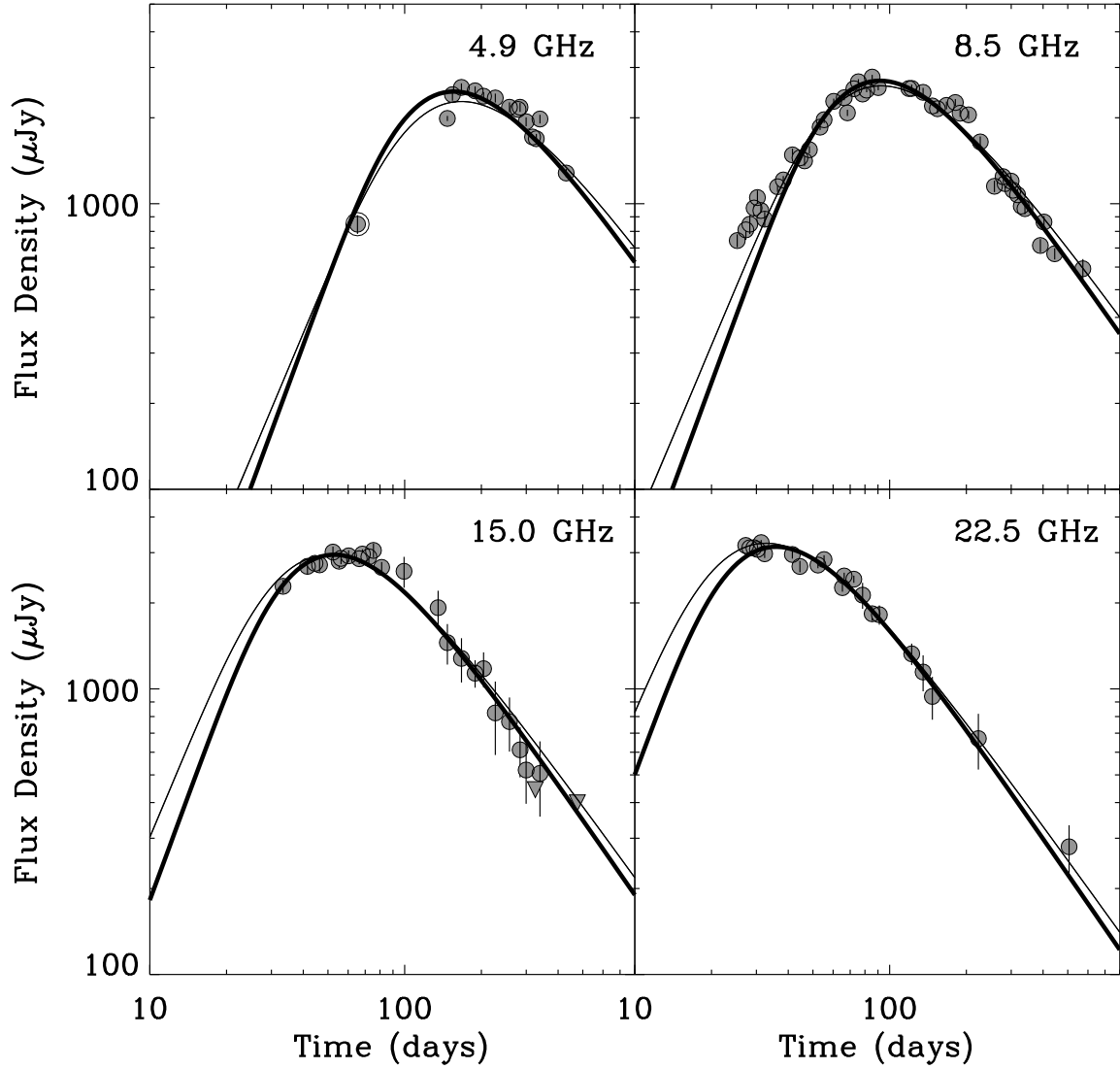


Fig. 2.— Radio light-curves of for the Type Ic SN 2003L were taken with the VLA at frequencies 4.9, 8.5, 15.0, and 22.5 GHz between January 2003 and July 2004. The single VLBA observation (5 GHz) is shown as an encircled dot. SSA Model 1 (thick solid line), and Models 2 and 3 (thin solid line) as described in §5 are over-plotted.

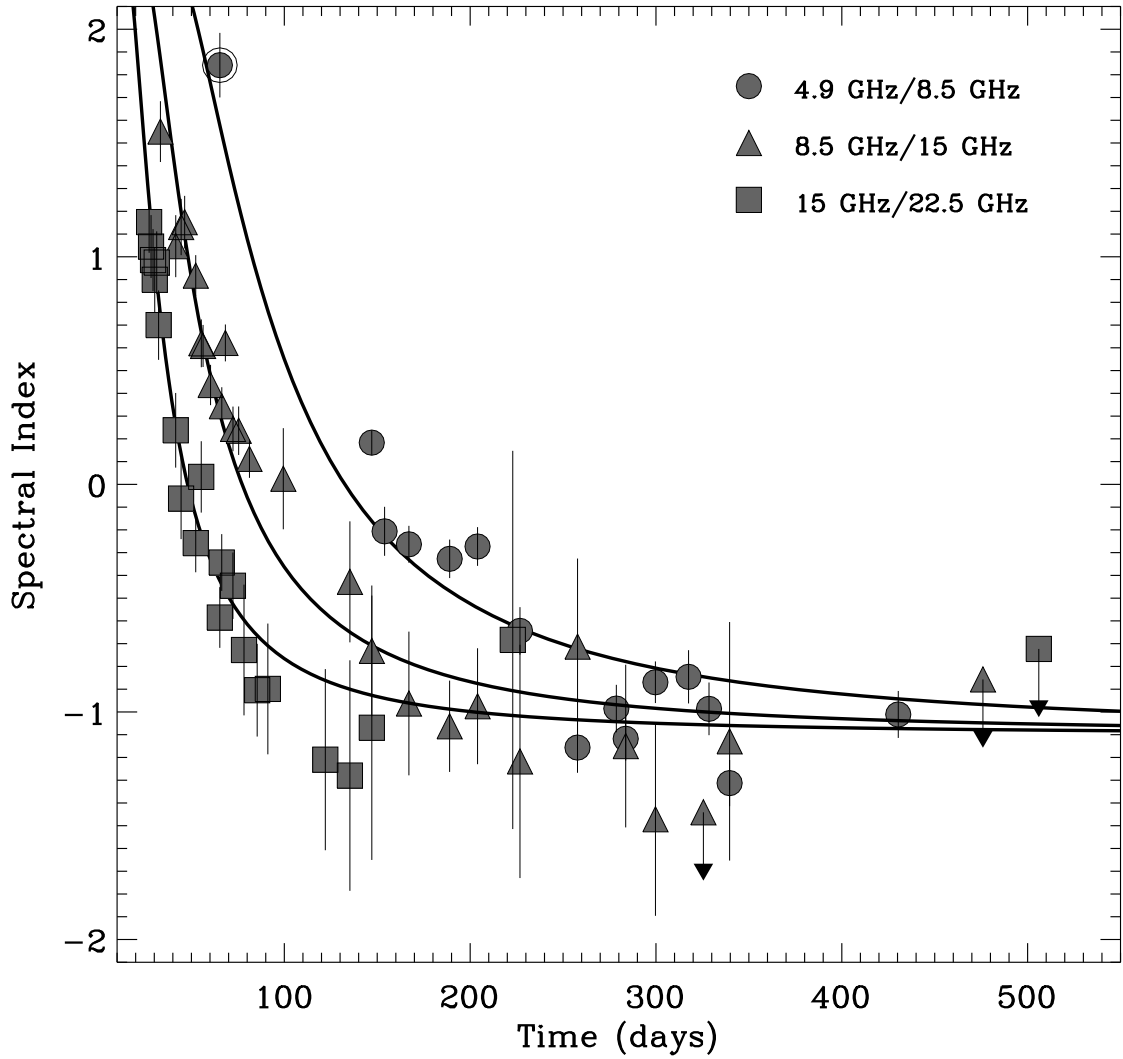


Fig. 3.— Spectral indices for the radio emission of SN 2003L. The temporal evolution of 4.9/8.5 GHz, 8.5/15.0 GHz, and 15.0/22.5 GHz spectral indices are shown and SSA Model 1 (§5) is over-plotted. We highlight the VLBA observation with an encircled dot.

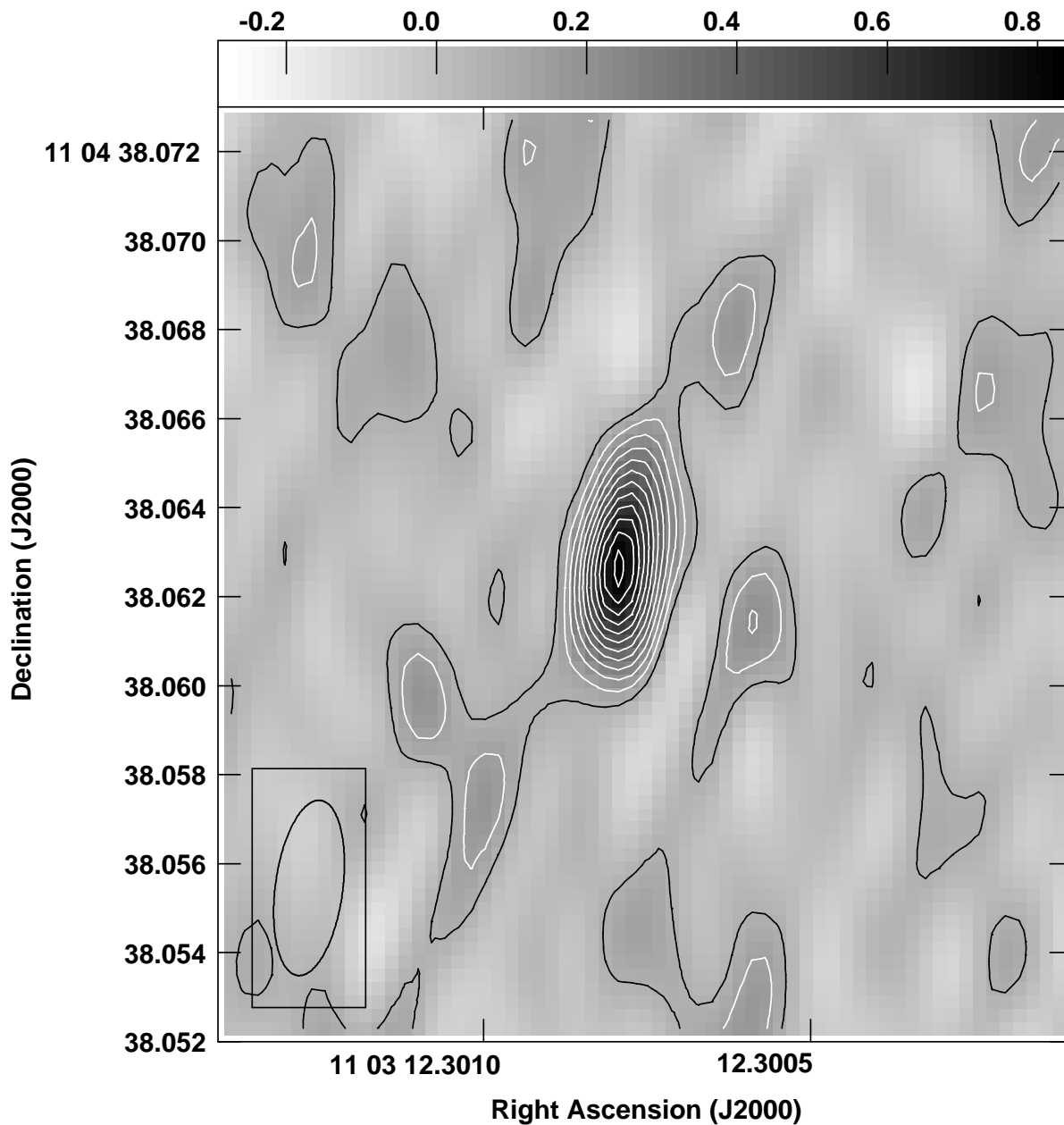


Fig. 4.— VLBA image of SN2003L at 4.9 GHz at $t \approx 65$ days after the explosion. We find a flux density for the supernova of $F_{4.9 \text{ GHz}} = 848 \pm 64 \mu\text{Jy}$ within a 3.158×1.285 mas beam. Contours define 1σ increments of $67 \mu\text{Jy}$. At a distance of 92 Mpc, this unresolved VLBA detection places a direct constraint on the size of the expanding ejecta of $r \lesssim 9.1 \times 10^{17}$ cm at $t \approx 65$ days.

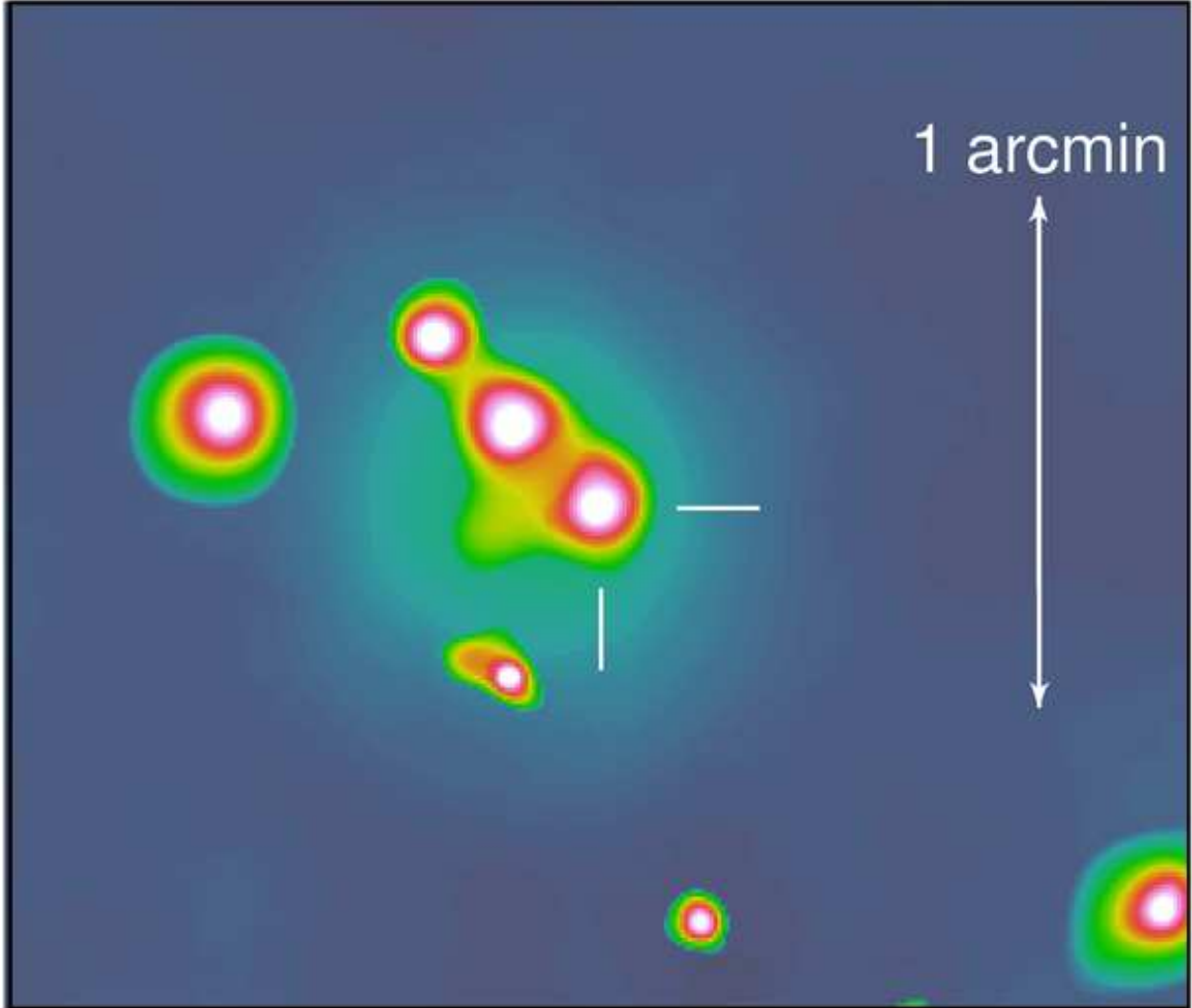


Fig. 5.— *Chandra* X-ray image of SN 2003L at $t \approx 40$ days. The 2–10 keV luminosity of SN 2003L is $L_X \approx 9.2 \times 10^{39}$ erg/s/Hz for a power-law spectral model. SN 2003L is therefore the most luminous X-ray SN Ibc (on this timescale) with the exception of SN 1998bw.

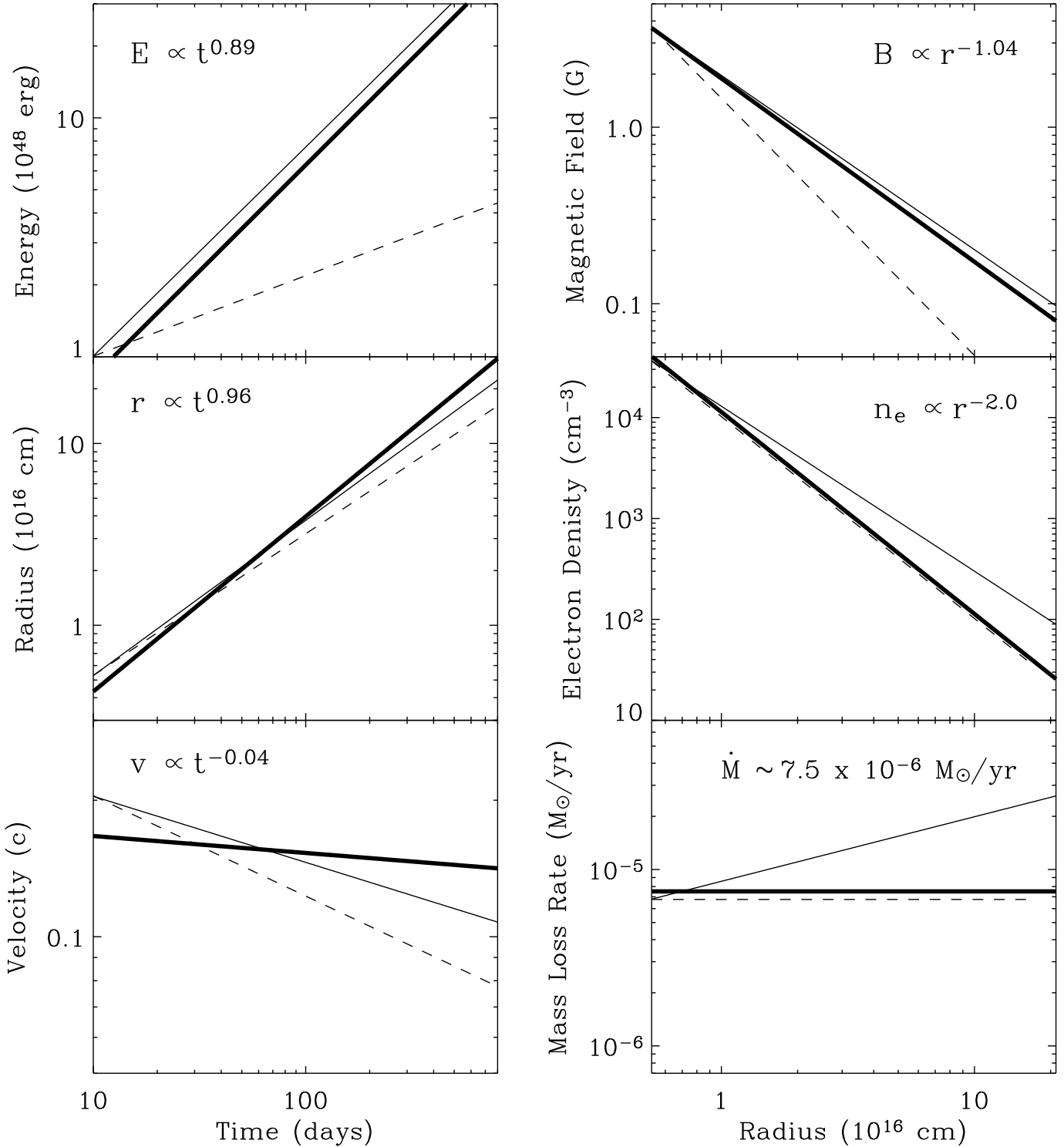


Fig. 6.— Physical parameters for SN 2003L based on SSA Model 1 (thick solid line), Model 2 (thin solid line) and Model 3 (thin dashed line) as described in Section 5. Left column: the temporal evolution from $t = 10 - 800$ days is shown for the ejecta energy, shock radius and average velocity (top to bottom). Right column: the radial profile of the magnetic field, electron number density and mass loss rate are shown from $r = 5 \times 10^{15}$ to 2.1×10^{17} cm. The scalings appearing at the top of each plot correspond to Model 1.

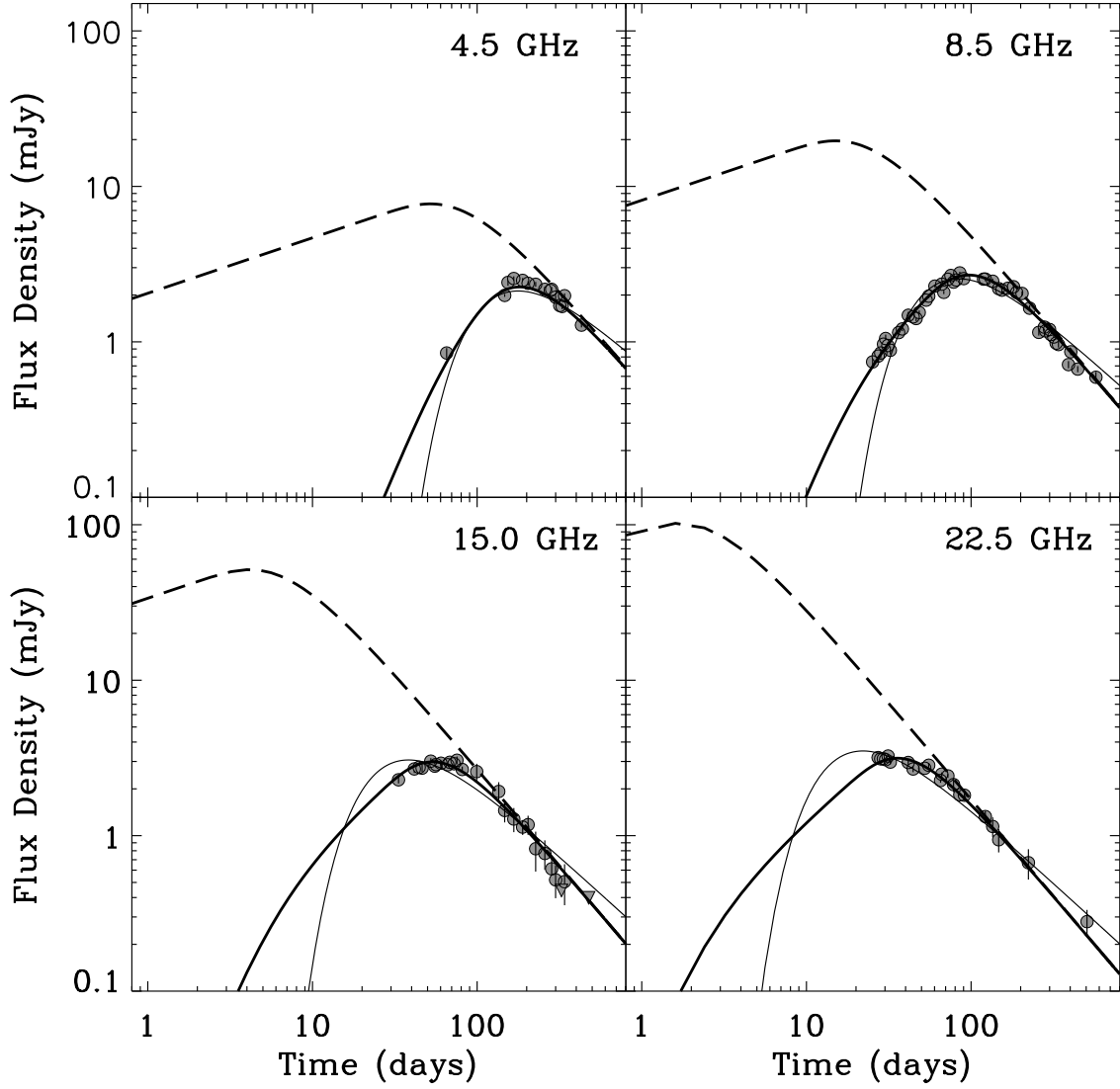


Fig. 7.— Free-free absorption fits for SN 2003L based on formalism from Weiler *et al.* (1986) (basic model; thin solid line) and Weiler, Panagia & Montes (2001) (complex model; solid line). The basic model provides a poor fit to the data while the complex model provides a significantly better fit by including additional absorption processes. The intrinsic (de-absorbed) synchrotron spectrum of the complex model (dashed line) implies a relativistic velocity which violates the VLBA constraint at $t \approx 65$ days.